

New Observational Metrics of Convective Self-Aggregation: Methodology and a Case Study

Toshiki KADOYA

Graduate School of Environmental Studies, Nagoya University, Nagoya, Japan

and

Hirohiko MASUNAGA

Institute for Space-Earth Environmental Research, Nagoya University, Nagoya, Japan

(Manuscript received 5 October 2017, in final form 1 August 2018)

Abstract

A new observational measure, the Morphological Index of Convective Aggregation (MICA), is developed to objectively detect the signs of convective self-aggregation on the basis of a simple morphological diagnosis of convective clouds in satellite imagery. The proposed index is applied to infrared imagery from the Meteosat-7 satellite and is assessed with sounding-array measurements in the tropics from Cooperative Indian Ocean Experiment on Intraseasonal Variability in the Year 2011 (CINDY2011)/Dynamics of the Madden Julian Oscillation (MJO) (DYNAMO)/Atmospheric Radiation Measurement (ARM) MJO Investigation Experiment (AMIE). The precipitation events during the observational period are first classified by MICA into “aggregation events” and “nonaggregation events”. The large-scale thermodynamics implied from the sounding-array data are then examined, with a focus on the difference between the two classes. The composite time series show that drying proceeds over 6–12 h as precipitation intensifies in the aggregation events. Such drying is unclear in the nonaggregation events. The moisture budget balance is maintained in very different manners between the two adjacent sounding arrays for the aggregation events, in contrast to the nonaggregation events that lack such apparent asymmetry. These results imply the potential utility of the proposed metrics for future studies in search of convective self-aggregation in the real atmosphere.

Keywords convective self-aggregation; tropical meteorology; satellite remote sensing; ground-based observations

1. Introduction

It has been found in radiative-convective equilibrium (RCE) simulations that when certain conditions are met, a random ensemble of convective clouds become localized or aggregate into a single cluster, a phenomenon that is known now as convective self-

aggregation (Held et al. 1993; Tompkins 2001; Bretherton et al. 2005). Self-aggregation proceeds with a dramatic change in the thermodynamic fields consisting of an expanding dry area with few cold clouds and a moist precipitating area being increasingly confined into a smaller domain. These processes, characteristic of convective self-aggregation, are explained in terms of various physical feedbacks. Bretherton et al. (2005) found that convective-water-vapor-radiation feedbacks are important for the progression of convective self-aggregation. Cloud radiative effects are another key factor for self-aggregation owing to the shallow

Corresponding author: Toshiki Kadoya, Graduate School of Environmental Studies, Nagoya University, Furo-cho, Chikusa-ku, Nagoya 464-8601, Japan
E-mail: kadoya@satellite.isee.nagoya-u.ac.jp
J-stage Advance Published Date: 24 August 2018



circulation caused by radiation cooling at the top of clouds, as demonstrated with a cloud-resolving model (Muller and Held 2012) and a general circulation model (Coppin and Bony 2015). Wing and Emanuel (2014) and Wing et al. (2017) quantitatively evaluated the physical mechanism of self-aggregation and found that the feedbacks among shortwave radiation, long-wave radiation, and surface fluxes play an important role, and the energy convergence due to horizontal transport strongly acts as positive feedback during the intermediate stages of the aggregation process. In order to investigate the validity of idealized simulations of self-aggregation, Holloway (2017) performed a set of sensitivity experiments with a realistic configuration to compare with idealized simulations. They confirmed that the aggregation mechanisms, as identified in the idealized simulations, are overall useful for analyzing the real atmosphere as well.

The signs of convective self-aggregation have been searched for also in observations. Tobin et al. (2012, 2013) studied the dependence of tropospheric relative humidity and outgoing longwave radiation on the degree of convective aggregation in satellite observations and found that those features are consistent with the results from existing numerical simulations, as reviewed above. Stein et al. (2017), investigating the observed relationship between convective aggregation and the vertical structure of clouds, discovered systematic behaviors in support of some known aspects of convective self-aggregation.

However, the observational evidence for convective self-aggregation is limited, and it remains unclear to what extent the known aspects of convective self-aggregation, as identified by idealized simulations, are relevant to the real atmosphere (Holloway et al. 2017). In this study, we develop a new observational measure to detect convective self-aggregation in satellite infrared imagery and apply it to a case study with sounding-array observations in the tropics for assessing the potential utility of the proposed method.

The data and analysis framework used to conduct the study is described in Section 2. In Section 3, a new analysis method is proposed to detect the possible signs of convective aggregation from satellite snapshots. The results are presented in Section 4 and discussed further in Section 5. A summary is given in Section 6.

2. Data sources

The datasets are outlined in this section.

2.1 Geostationary meteorological satellite measurements

In order to track the temporal variability of convective clouds, the brightness temperature dataset from the *Meteosat-7* Channel 8 (10.5–12.5 μm) measurements is analyzed. *Meteosat-7* is a European meteorological satellite that was launched to fly over 0° in longitude in 1997 but was moved to 57.5°E in 2006. From July 2006 until March 2017, *Meteosat-7* has been operated to acquire data capturing the entire Indian Ocean ($25\text{--}115^\circ\text{E}$, $45^\circ\text{S}\text{--}45^\circ\text{N}$). The current target area is $72\text{--}81^\circ\text{E}$ and $8^\circ\text{S}\text{--}7^\circ\text{N}$, a domain just covering the in situ observational area described below, with a 30 min temporal resolution and $0.045^\circ \times 0.045^\circ$ spatial resolution. In this study, convective clouds are identified by a constant threshold applied to infrared brightness temperature. The threshold value is chosen, according to the previous studies (e.g., Maddox 1980; Roca and Ramanathan 2000), to be 240 K.

2.2 Sounding observations

The atmospheric thermodynamic field is analyzed using the radiosonde observation network from the Cooperative Indian Ocean Experiment on Intraseasonal Variability in the Year 2011 (CINDY2011)/Dynamics of the Madden Julian Oscillation (MJO) (DYNAMO)/Atmospheric Radiation Measurement (ARM) MJO Investigation Experiment (AMIE) (Yoneyama et al. 2013). This field campaign was carried out in the Indian Ocean region near the equator during the period from late 2011 to early 2012. The observational stations were deployed to form two sounding networks straddling the equator, that is, the northern sounding array (NSA) and the southern sounding array (SSA), comprised of six sounding stations (see Fig. 1, top). In this study, we used the Colorado State University (CSU) array-averaged (i.e., averaging from the soundings consisting of each array) analysis product version 3a (Johnson and Ciesielski 2013) and the area-averaged precipitation of TRMM 3B42v7 product, with averaging applied to all quarter-degree grid boxes within each array. Representativeness issues potentially arising from sporadic station samples will be briefly discussed in Section 5. The column radiative heating stored in the CSU DYNAMO product is originally taken from the Clouds and the Earth's Radiant Energy System (CERES) data product. In this analysis, precipitation, water-vapor mixing ratio, radiative heating, and moisture budget parameters (the vertically integrated moisture tendency, horizontal advection, vertical advection, and budget-derived rainfall) are used from the CSU

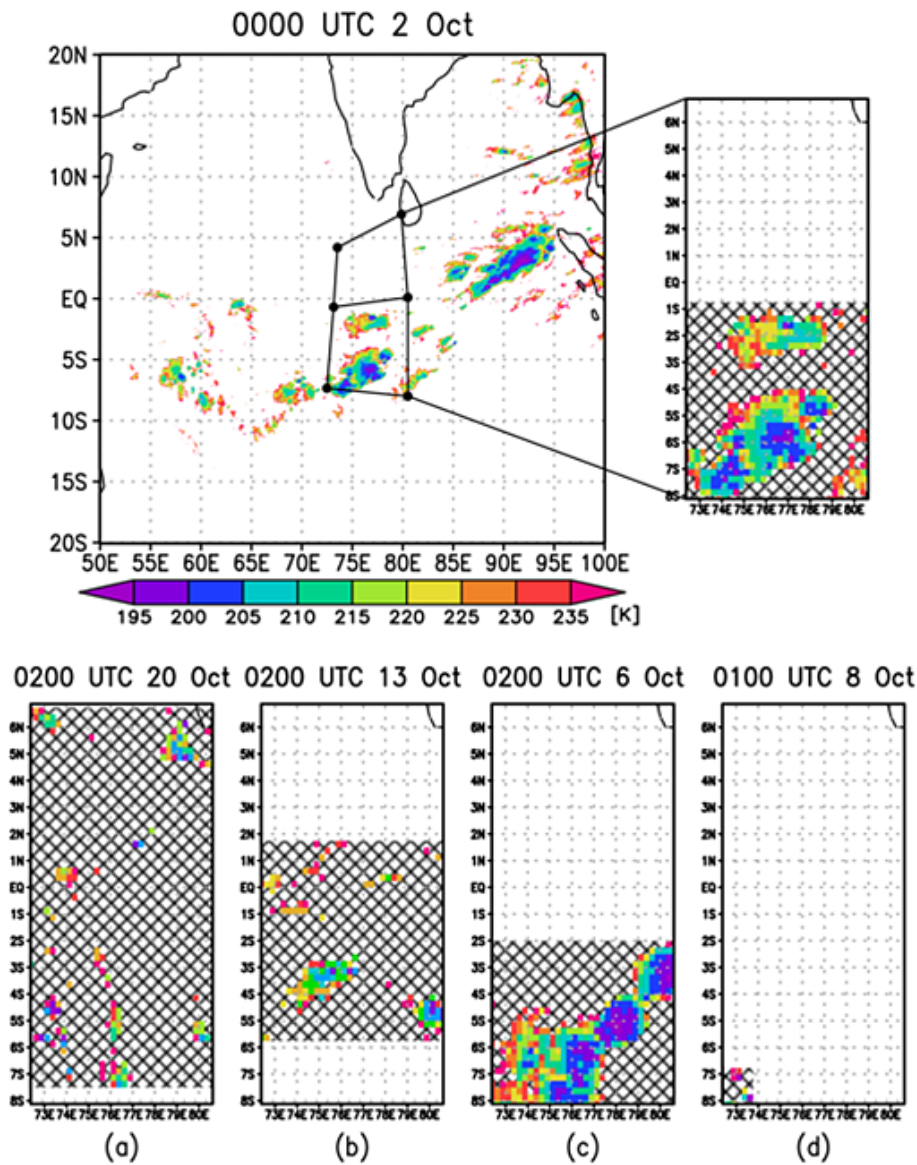


Fig. 1. Top. Snapshot of brightness temperature from Meteosat-7 infrared data at 0000 UTC 2 Oct 2011. The rectangular area indicates the analysis domain of this study with the DYNAMO/CINDY2011/AMIE sounding arrays also shown. The right figure is an enlarged view of the analysis region. The hatched area shows the convective area and the nonhatched area shows the clear-sky area. Bottom. Four example snapshots: (a) 0200 UTC 20 Oct 2011, MICA = 0.00238, SCAI = 13.6; (b) 0200 UTC 13 Oct 2011, MICA = 0.0555, SCAI = 7.72; (c) 0200 UTC 6 Oct 2011, MICA = 0.215, SCAI = 0.872; (d) 0100 UTC 8 Oct 2011, MICA = 0.212, SCAI = 0.251.

DYNAMO product. The analysis period is three months, from October 1, 2011, to December 31, 2011, and the observational time interval is 3 h.

3. Analysis framework

Tobin et al. (2012, 2013) devised the Simple Con-

vective Aggregation Index (SCAI) as an indicator of aggregation, which is a parameter that combines the number of cloud clusters (N) and the mean distance between the clusters (D_0):

$$\text{SCAI} = \frac{N}{N_{\max}} \frac{D_0}{L} \times 1000,$$

$$D_0 = \sqrt{\prod_{i=1}^n d_i},$$

$$n = N(N-1)/2.$$

Here, N_{\max} is the maximum possible number or half the total number of pixels occupying the study area and L is the length scale of this area. SCAI shows the degree of disaggregation; that is, SCAI is smaller where cloud clusters are more aggregated. However, as Tobin et al. (2012) pointed out, SCAI by design requires multiple cloud clusters to exist in the observed region, and SCAI is ill-defined in cases where the number of cloud clusters is 0 or 1 since $N = 0$ and $D_0 = 0$, respectively. In addition, SCAI is practically a measure of the number of cloud clusters, as confirmed later, and does not explicitly reflect the areal extent of clear sky, which is one of the remarkable features of self-aggregation. The predominance of clear sky in an aggregated state is not directly considered for other proposed metrics of the degree of convective aggregation either, including the organization index (Tompkins and Semie 2017) and the convective organization potential (COP) (White et al. 2018). In this study, we devised a new index of convective self-aggregation, with these issues taken into account.

3.1 Morphological Index of Convective Aggregation (MICA)

In this study, the following equation is proposed as an index for the degree of self-aggregation:

$$\text{MICA} = \frac{\sum_i S_{c,i}}{A_{\text{cls}}} \times \frac{[A_{\text{obs}} - A_{\text{cls}}]}{A_{\text{obs}}}.$$

Here, A_{obs} is the total observed area, A_{cls} is the area enclosed by the smallest possible rectangle that can be drawn around all cloud clusters in the domain, and $S_{c,i}$ is the area of the i th cloud cluster or the contiguous area with infrared brightness temperatures below 240 K. This nondimensional index, hereafter called the Morphological Index of Convective Aggregation (MICA), is intended to measure the degree of convective aggregation, with a higher value representing a higher degree of aggregation. As reviewed in Section 1, convective self-aggregation proceeds as convective clouds aggregate into a limited number of large cloud clusters in a small confined area, while the clear-sky area expands further. Therefore, in MICA, the degree of aggregation is quantitatively evaluated by how

densely cloud clusters are aggregated into a confined area ($\sum_i S_{c,i}/A_{\text{cls}}$) and, at the same time, by how much area the clear sky outside the aggregated convective area occupies relative to the whole observed domain ($[A_{\text{obs}} - A_{\text{cls}}]/A_{\text{obs}}$). Both of these elements increase as the aggregation proceeds, and indeed MICA exhibits a large value indicative of convective aggregation only when these two parameters show high values simultaneously. Otherwise, MICA stays minimal, with the result of either of these factors being small.

In order to visually demonstrate the performance of MICA, MICA is applied to selected convective events in Fig. 1 (top). The observational domain (A_{obs}) is a rectangle of $9^\circ \times 15^\circ$ or roughly $1,000 \text{ km} \times 1,700 \text{ km}$ in size, which is comparable to or larger than the computational domain typical of RCE simulations conducted in existing convective aggregation studies. In this particular example, A_{cls} is represented by a hatched square, which is confined to the lower half of the observed domain (considered as an aggregated state). Figure 1 (bottom) shows the results of MICA and SCAI applied to a few cases with different cloud distributions. When convective clouds are sporadic across the whole area (Fig. 1a), MICA becomes small (a, MICA = 0.00238) supposedly owing to the large A_{cls} expected from the widely spread cloud clusters. In this case, SCAI is as high as 13.6, which implies a disaggregated state as well. As aggregation progresses (Figs. 1b, c), MICA turns out to be a large value (b, MICA = 0.0555, SCAI = 7.72; c, MICA = 0.215, SCAI = 0.872). These examples demonstrate that MICA can characterize the clumping state of cloud clusters as SCAI does. However, MICA does not work as intended in cases where there is one cloud cluster covering the whole area, or in other extreme cases where a few small cloud clusters happen to be found in one corner of the observed domain that is otherwise clear (as in Fig. 1d). In the former case, MICA becomes 0 because a clear-sky area is required by MICA to always accompany aggregation. If the observed region is set to be sufficiently large, however, such situations can be practically eliminated. In the latter case, the index value increases for a false reason (d, MICA = 0.212, SCAI = 0.251), making it impossible to distinguish from the bona fide aggregation. Although this case is rather rare, it is difficult to exclude mechanically from MICA only. MICA will not work properly either when an “outlier” exists in the farthest corner of the domain from the main group of clumped clusters, in which case $[A_{\text{obs}} - A_{\text{cls}}]/A_{\text{obs}}$ would be nearly 0 for a potentially aggregated state. For these reasons, it is necessary to omit the cases

where the cloud amount in the observational region is extremely close to 0 or 1, and it is desirable as well to use independent quantities such as precipitation or cloud coverage together with MICA as a reference to avoid erroneous estimates. Unlike SCAI, MICA does not evaluate the randomness of convective distribution, but MICA has a unique advantage of fully exploiting the morphological properties of satellite infrared imagery including nonprecipitation regions.

3.2 Compositing analysis

In order to investigate the temporal variability of MICA and meteorological parameters associated with the possible occurrence of convective self-aggregation, a composite analysis is performed in the manner described as follows. Figure 2 shows the complete time series of the array-averaged rainfall

from the TRMM 3B42v7 product, MICA, SCAI, and the number of convective clusters for a three-month period. MICA is plotted upside down so it compares directly with SCAI, with the downward direction indicating a higher degree of aggregation. While SCAI is clearly influenced by three MJO episodes (Yoneyama et al. 2013), MICA exhibits no sign of intraseasonal modulation because the clear-sky term, considered as a signal of aggregation in MICA, stays very small within MJO convective envelopes. Nevertheless, MICA and SCAI overall agree in that convective aggregation tends to proceed in early October, early December, and late December, all during the inactive phases of the MJO. On the other hand, only SCAI finds spells of aggregation in early and middle November. This discrepancy is practically insignificant because these periods do not contain major

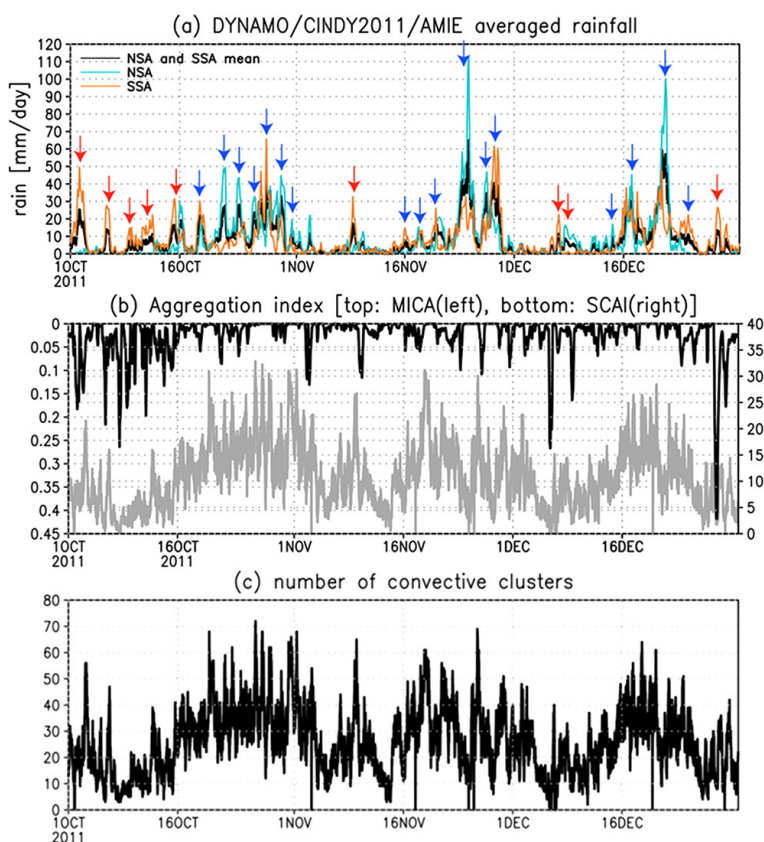


Fig. 2. Time series of (a) DYNAMO/CINDY2011/AMIE averaged rainfall over the total NSA + SSA domain (black), (b) aggregation index MICA (black, labeled on the left) and SCAI (gray, labeled on the right) with MICA plotted upside down, and (c) the number of convective clusters for the same region. The light-blue line and orange line indicate DYNAMO NSA-averaged precipitation and DYNAMO SSA-averaged precipitation, respectively. The arrows in (a) show the aggregation (red) and nonaggregation (blue) events, classified according to the method described in Section 3.

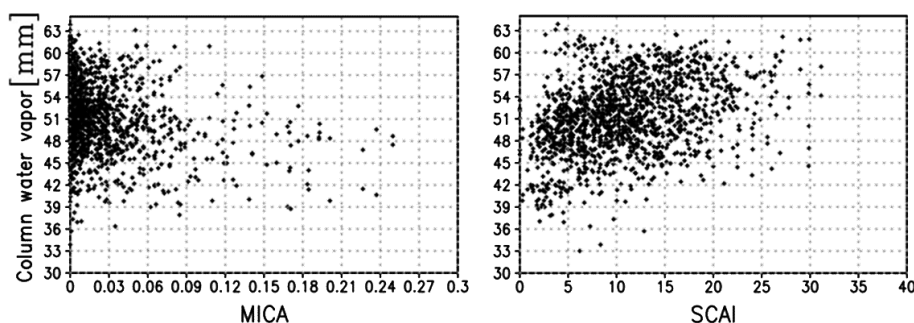


Fig. 3. Scatter diagram of the relationship between the aggregation index (left: MICA; right: SCAI) and column water vapor.

precipitation events in any case (Fig. 2a). Figures 2b and 2c show that SCAI closely traces the number of cloud clusters as expected from the way it is defined (Tobin et al. 2012). Figure 3 shows the relationship between MICA/SCAI and the array-averaged column water-vapor mixing ratio during the whole observation period. This provides evidence that MICA and SCAI each suggest a negative correlation between moisture and the degree of aggregation (recall that SCAI decreases as aggregation advances) as known from previous studies, although the spread is so large that the systematic correlation is marginal.

The ± 24 h time sequence is sampled around each precipitation peak (time = 0) on the basis of MICA and then classified as either “aggregation events” or “nonaggregation events”. It is noted that this nomenclature remains tentative until MICA is proven firmly in future investigations to be a reliable measure of self-aggregation as known from the literature. The extracted time series are composited into a statistical time series representing each of the aggregation and nonaggregation events. Here, the aggregation events are defined at the precipitation peak when $\text{MICA} \geq 0.1$ and precipitation $\geq 5 \text{ mm day}^{-1}$ (red arrows in Fig. 2a), and the nonaggregation events are identified with $\text{MICA} < 0.1$ and precipitation $\geq 5 \text{ mm day}^{-1}$ (blue arrows in Fig. 2a). The precipitation peaks are first sought individually in the NSA- and SSA-averaged rainfall, and if multiple peaks from either array are present within consecutive ± 24 h, only the highest among them is selected. Precipitation peaks lower than 5 mm day^{-1} are not used for the composite analysis. We repeated the analysis by changing the threshold definitions within a plausible range and confirmed that it does not qualitatively affect the subsequent discussions (not shown). By this method, 9 aggregation events and 17 nonaggregation events are obtained.

Figure 4 shows snapshots of all the extracted aggregation events at the hour of peak precipitation. These snapshots show that major, if not whole, portions of aggregated clouds and the surrounding clear-sky areas are overall captured by the sounding arrays, giving credibility to the thermodynamic budget analysis presented later at least around the time of peak activity. It is not ensured, however, whether the same argument holds over an extended period of time because convective systems often move into and out of the study domain as they develop and dissipate on their own. Cloud clusters traversing the domain could introduce misleading signals in the statistics, although the key physical signatures intrinsic to the convective dynamics would not be entirely lost by including propagating convective systems together in the composite (Masunaga 2015).

It may be noteworthy that the aggregation events identified in this work prefer relatively quiescent periods not heavily disturbed by frequent intrusions of cloud clusters. While systematic zonal propagation of disturbances into the study domain is evident during three MJO passages as noted earlier (Fig. 5a), such extensive zonal propagation is less clear outside the MJO convective envelopes. No clear signal of meridional propagation is found at any time (Fig. 5b). With the exception of the November 9th event, which probably belongs to a propagating system, most of the convective events outside the active MJO phase are unlikely to be totally aliased by external disturbances that accidentally traverse the study domain. Given that the aggregation events detected in the study are mostly outside the active phases of MJO (Fig. 2a), it would not be very likely that convective aggregation as discussed here is heavily affected by advection from the neighboring regions. With that being said, the possible effects of propagating systems on the interpretation

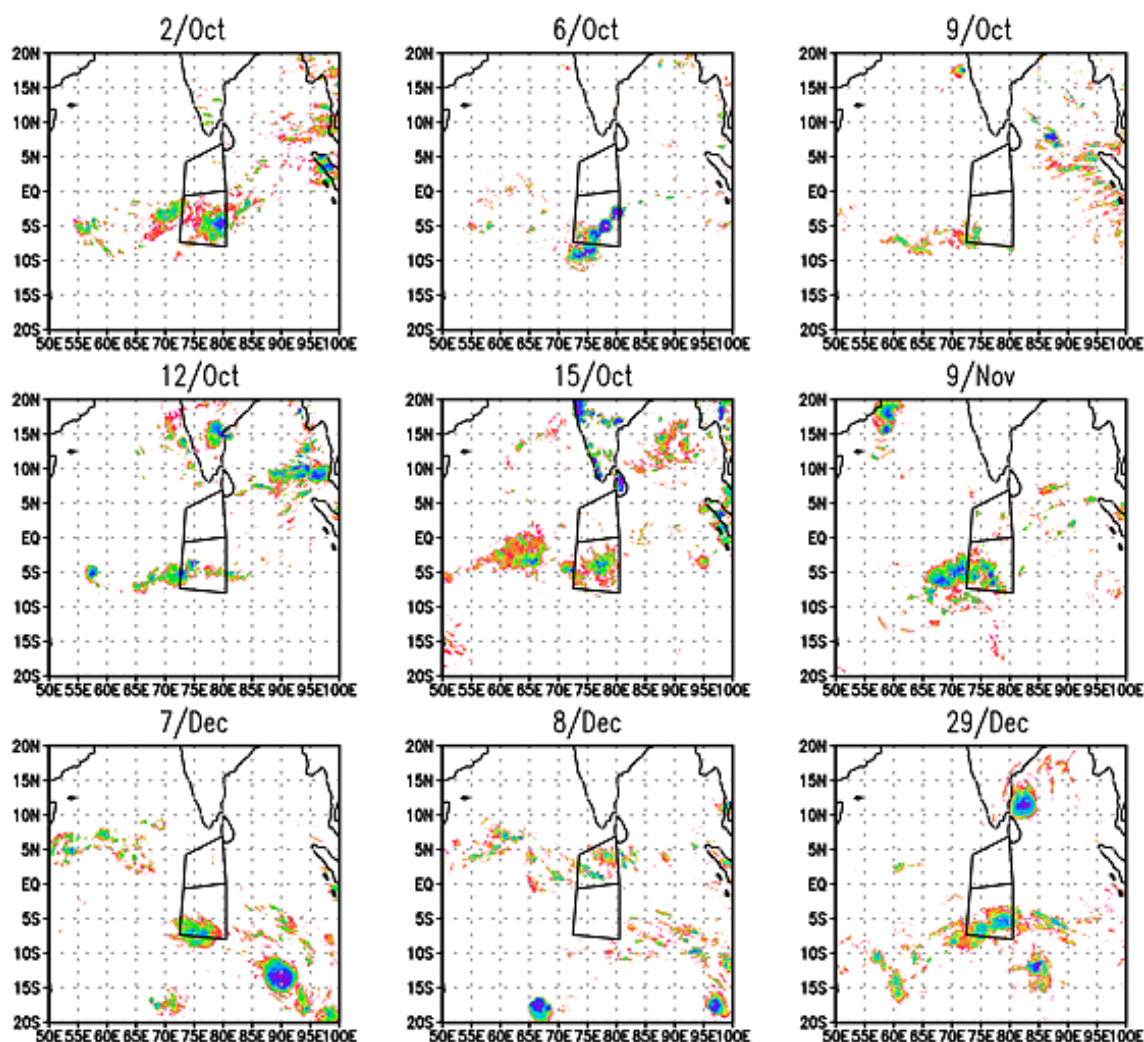


Fig. 4. Snapshots of infrared brightness temperature for all nine observed aggregation events at the time of peak precipitation.

of MICA are not fully sorted out by the present observations alone and have yet to be examined further elsewhere.

4. Results

Figure 6a shows the composite time series of MICA for the aggregation events (red line) and for the nonaggregation events (blue line). For the aggregation events, a conspicuous increase in MICA is observed toward the hours of peak precipitation, with the amplitude ranging over an order of magnitude from 0.01 to above 0.1. For the nonaggregated precipitation event, on the other hand, MICA stays small by definition. This confirms that the aggregation events are isolated

from the nonaggregation events as effectively as intended. It is noted that the variation of MICA for the aggregation events is confined within ± 12 h around the precipitation peak time (at 0 h). This time scale may be set either by a local development of convective systems or by propagating systems entering and leaving the study domain, so it is unclear for the moment whether it physically represents the aggregation processes. If this time scale is actually relevant to the aggregation in nature, it contrasts with the previous studies based on numerical simulations, where convective self-aggregation makes progress more slowly over a few weeks to several tens of days (Holloway et al. 2017).

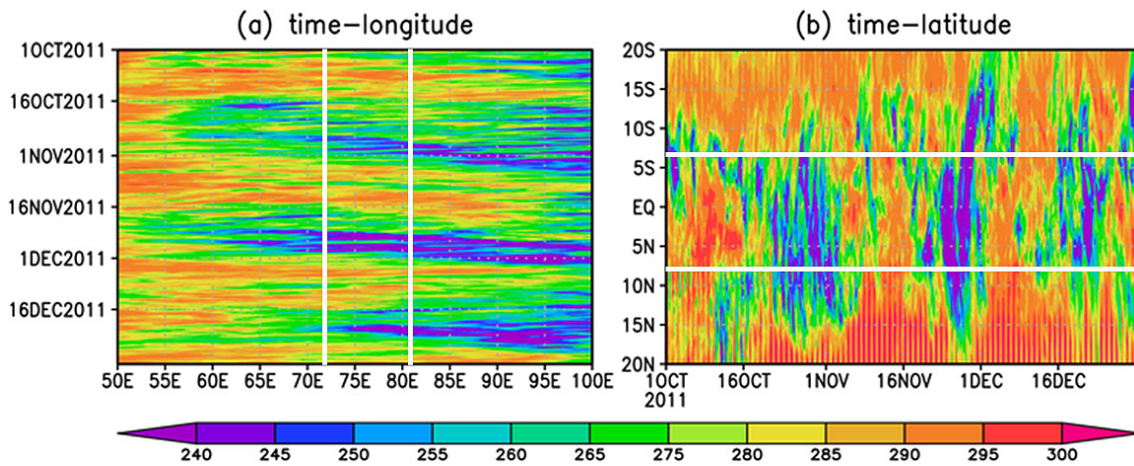


Fig. 5. (a) Time-longitude (averaged over 8°S–7°N) and (b) time-latitude (averaged over 72–81°E) sections of infrared brightness temperature. The area bound between two white lines or 72–81°E in (a) and 8°S–7°N in (b) indicates the observed region to define MICA.

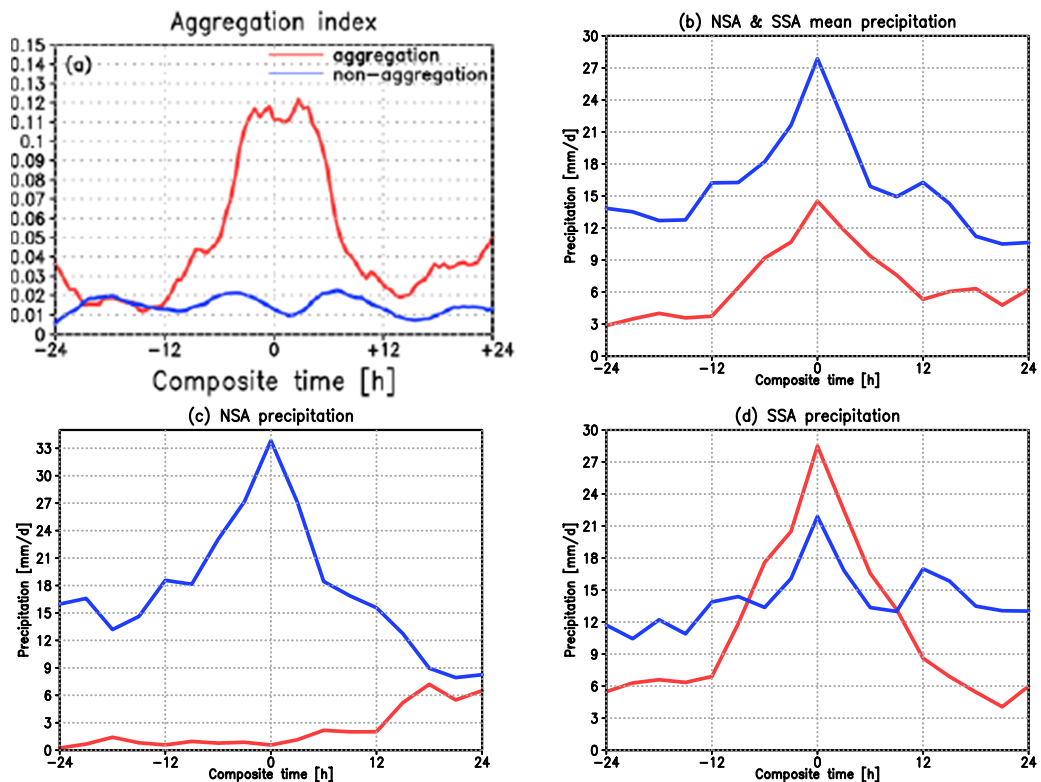


Fig. 6. Composite time series of (a) the aggregation index MICA, (b) DYNAMO/CINDY2011/AMIE averaged rainfall over the total NSA + SSA domain, (c) DYNAMO NSA-averaged precipitation, and (d) DYNAMO SSA-averaged precipitation for the aggregation (red line) and nonaggregation (blue line) events. The time axis spans 24 h before and after the time of precipitation peak at $t = 0$. Note that the range of precipitation varies among panels (b)–(d). All aggregation and nonaggregation events for (a) and (b), while aggregation events are sampled only from the cases where convection resides in SSA for (c) and (d).

In Fig. 2a, precipitation averaged within NSA (light-blue line) and SSA (orange line) is shown together with the mean of these two (black line). For the aggregation events (red arrows in Fig. 2a), precipitation is localized in either NSA or SSA most of the time, whereas in the nonaggregation events (blue arrows in Fig. 2a), precipitation occurs simultaneously in both NSA and SSA in most cases. This is as expected from the definition of MICA, designed to embody the horizontal concentration of precipitation characteristic of self-aggregation. The domain-mean or NSA-and-SSA-combined precipitation (Fig. 6b) shows that the nonaggregation events produce significantly heavier rainfall than the aggregation events. This contrast virtually reflects the MJO variability because the aggregation events prefer the dry phases of MJO. Ideally, it is desirable for a fair comparison to sample the aggregation and nonaggregation events that fall in a similar precipitation range, but this is not feasible for the limited samples of this work. Figures 6c and

6d show the composite time series of precipitation in NSA and SSA during aggregation (red) and nonaggregation (blue). Because precipitation is mostly localized in SSA (see Figs. 2a, 4), the composite analysis hereafter (Figs. 6c, d, 9) excludes the case of December 8 where precipitation dominates NSA for clarity of presentation. As a result, precipitation is virtually absent in NSA for the aggregation events, making a sharp contrast to the nonaggregation events showing a distinct peak at $t = 0$. The precipitation evolution for the nonaggregation events, though qualitatively similar, differs in magnitude by 50 % at the peak between NSA and SSA. In SSA, the rainfall evolves over time in a similar manner, although the amplitude of variability is greater in the aggregation events than in the nonaggregation events.

Figure 7 shows the composite time series of the water-vapor mixing ratio anomaly defined against the temporal average during ± 24 h. Figures 7a and 7c show NSA and SSA for the aggregation events, and

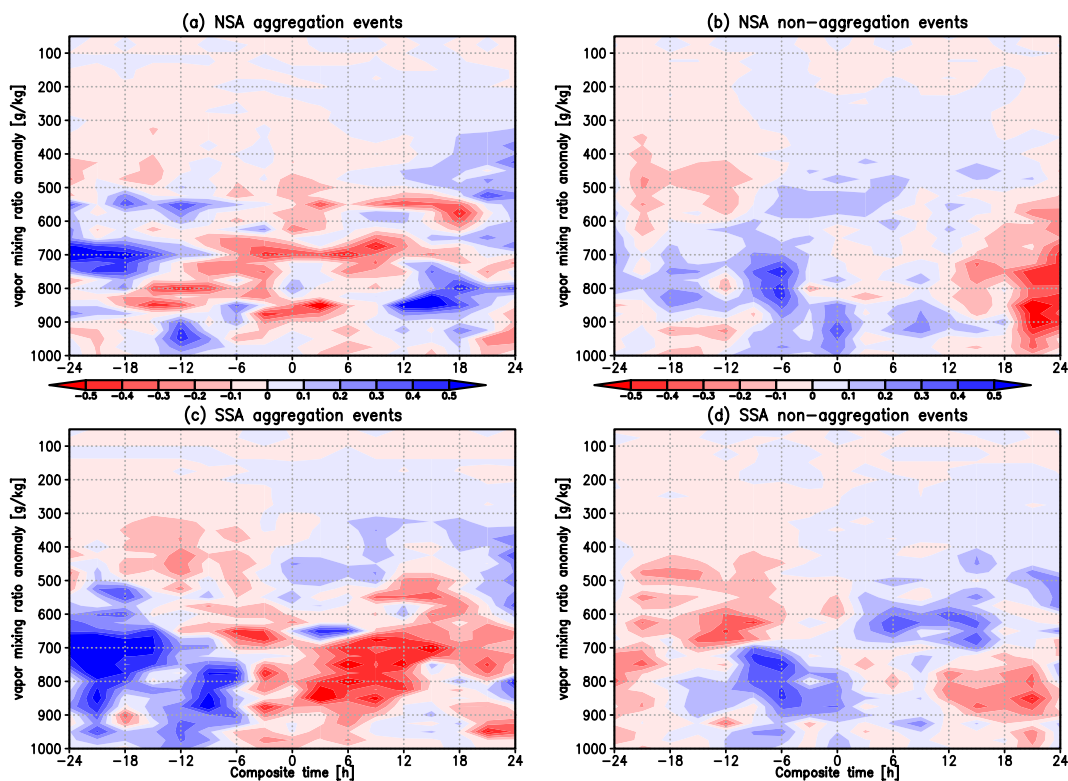


Fig. 7. Composite time series of water-vapor mixing ratio anomaly (g kg^{-1}) with respect to the average over all composite times (± 24 h) from DYNAMO NSA (a, b) and DYNAMO SSA (c, d) for the aggregation or nonaggregation events. For the aggregation events, only the cases where precipitation is localized in SSA are included in the analysis. Panels (a) and (c) use SSA only aggregation events. Panels (b) and (d) use all nonaggregation events.

Figs. 7b and 7d present the two sounding arrays for the nonaggregation events. Nonaggregation precipitation systems (Figs. 7b, d) accompany a moist anomaly during 12 h before the precipitation. In the aggregation events, on the contrary, a dry anomaly persists in the midtroposphere for 6 h before and after the precipitation peak in both arrays (Figs. 7a, c). Drying before the precipitation peak is at odds with the known characteristics prior to developing precipitation in general (e.g., Sherwood 1999), but it does not contradict the expansion of the drying area accompanying convective self-aggregation. In order to investigate the potential factors responsible for the differences between the aggregation and nonaggregation events, we conduct a moisture budget analysis in the next section.

5. Discussion

5.1 Time variation of the water vapor and radiation fields

The midtropospheric moisture variability was found to exhibit contrasting behaviors between the aggregation and nonaggregation events. The possible factors controlling the observed water-vapor fluctuations are explored in terms of the moisture budget analysis. The vertically integrated large-scale moisture budget is written as follows:

$$\begin{aligned} \left\langle \frac{\partial L_v q}{\partial t} \right\rangle &= -\langle \mathbf{v} \cdot \nabla L_v q \rangle - \left\langle \omega \frac{\partial L_v q}{\partial p} \right\rangle - \langle Q_2 \rangle \\ &= -\langle \mathbf{v} \cdot \nabla L_v q \rangle - \left\langle \omega \frac{\partial L_v q}{\partial p} \right\rangle + L_v (E - P), \end{aligned}$$

where

$$\langle \cdot \rangle \equiv \frac{1}{g} \int_{p_r}^{p_{sf}} (\cdot) dp,$$

q is the water-vapor mixing ratio, L_v is the specific latent heat of vaporization, \mathbf{v} is the horizontal flow, ω is the vertical pressure velocity, Q_2 is the apparent moisture sink (Yanai et al. 1973), P is precipitation, E is the surface evaporation rate, g is the gravitational acceleration, p_{sf} is the surface pressure, and p_r is the top of the atmosphere chosen to be 50 hPa. Each term of the budget formula is calculated using the array-averaged radiosonde observations except for the Q_2 term. Since it is difficult to directly observe Q_2 , it is calculated as the residual once the other terms are given.

Figure 8 shows the results of the column-integrated water-vapor budget analysis. As mentioned above, the aggregation composite consists only of the cases

where the precipitation peak resides in SSA. In aggregation events, subtle drying is observed prior to the peak precipitation in NSA, whereas in SSA, notable drying spells appeared multiple times during the evolution. These drying events are driven mainly by lower- and midtropospheric variability, though not entirely in a coherent manner across altitudes (Fig. 7), which does not contradict the expansion of dry areas as known for the self-aggregation. The nonaggregation events experience notable moistening before $t = 0$, followed by a neutral or marginally drying spell (Figs. 8b, d). The horizontal advection of water vapor has little contribution to the moisture budget in all cases. This is in line with a previous study analyzing DYNAMO datasets, showing that the horizontal advection plays only a minor role in the moisture budget (Ruppert and Johnson 2015). Inoue and Back (2015) also confirmed the smallness of horizontal moisture advection for a short-time variability of one to two days, although horizontal advection can be important on intraseasonal time scales. However, care must be taken regarding the uncertainties in the horizontal advection estimates. The horizontal moisture advection could be erroneous when the horizontal moisture flux is poorly sampled by the limited number of stations consisting of the DYNAMO sounding arrays (Hannah et al. 2016).

On the other hand, the difference is evident in the vertical moisture advection between the aggregation and nonaggregation events. In the aggregation events (Figs. 8a, c), the vertical moisture advection remains small in NSA, whereas it grows significantly in SSA, confirming a vigorous development of convective clouds only in SSA (recall that we have selected the cases with convection residing in SSA only). Meanwhile, in the nonaggregation events (Figs. 8b, d), the vertical moisture advection has considerable magnitude in both NSA and SSA. Moistening owing to vertical advection is largely counteracted by Q_2 , leaving behind a small moisture tendency.

The vertical moisture advection term and Q_2 roughly counteract each other for the nonaggregation events. For the aggregation events in SSA, however, Q_2 does not precisely coincide with the vertical advection, resulting in a moisture budget imbalance that accounts for the negative moisture tendency mentioned earlier. It is suggested that efficient precipitation for the aggregation events temporarily exceeds moistening by vertical advection and causes drying. As such, drying is driven by moist convection itself for those events, whereas in the RCE experiments, the primary source of drying is the subsidence in the clear-sky region.

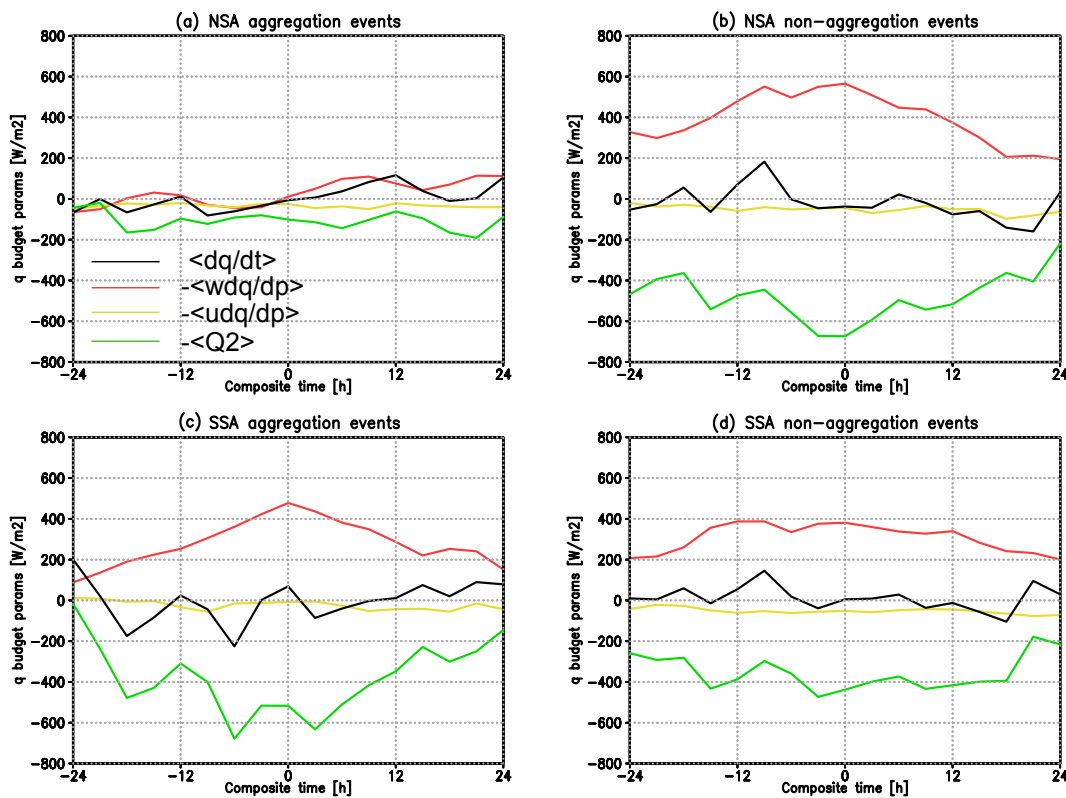


Fig. 8. Composite time series of vertically integrated moisture budget parameters (W m^{-2}) from DYNAMO NSA (a, b) and DYNAMO SSA (c, d) for the aggregation or nonaggregation event. Budget terms are calculated as shown in Section 5, with the Eulerian tendency (black), horizontal advection (yellow), vertical advection (red), and apparent sources (green). Panels (a) and (c) use SSA only aggregation events. Panels (b) and (d) use all nonaggregation events.

To examine the budget imbalance in light of the satellite-observed precipitation, Figs. 9a and 9b show the time series of TRMM 3B42v7 precipitation and Q_2 -derived precipitation in SSA for the aggregation events and nonaggregation events, respectively. The evaporation flux required for evaluating the Q_2 -derived precipitation is taken from the Woods Hole Oceanographic Institution product as stored in the CSU DYNAMO dataset. The Q_2 -derived precipitation captures a broad enhancement of rainfall but fails to reproduce a sharp peak as implied by the satellite observations. A plausible source of this discrepancy arises from uncertainties in the horizontal moisture advection as mentioned above. If the difference in precipitation in Fig. 9a is due to errors in the horizontal advection of water vapor, it is suggested that the excessive precipitation in Q_2 before -12 h should be attributed to drying by horizontal advection, while an underestimated precipitation around the precipitation

peak might imply moistening by horizontal advection, respectively. Although it is difficult to conclude that with confidence from the present data, the evolution of the aggregated events may be associated with moisture import to or moisture export from the precipitating atmospheric column, which is worthy of a future investigation in light of the similar dynamic processes known for convective self-aggregation. Figures 9c and 9d show the composite time series of radiative heating rates for each sounding array. The striking enhancement of radiative heating (or suppressed cooling) around $t = 0$ for aggregation events is explained presumably by the greenhouse effect of high clouds developing as precipitation intensifies. It may be aliased by the diurnal cycle of shortwave heating to some degree, but not entirely because the aggregation events currently sampled are not synchronized in local time and would not provide a clear $t = 0$ peak as observed by the diurnal solar cycle alone. The non-

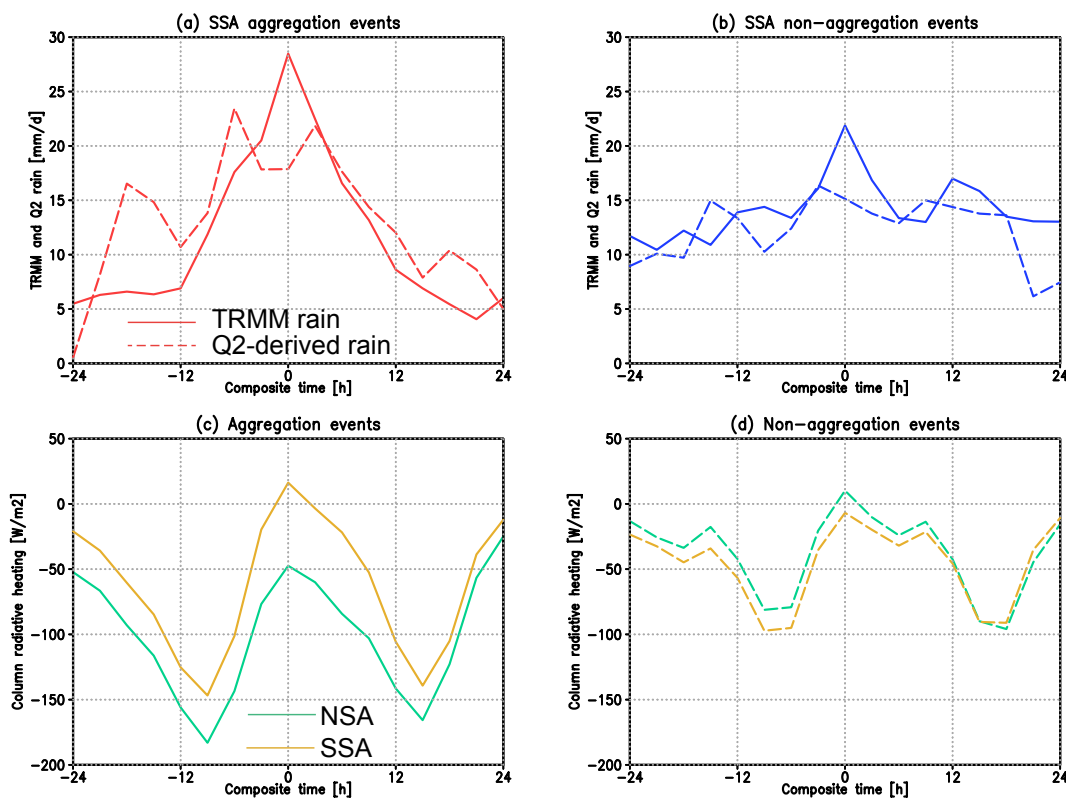


Fig. 9. Composite time series of (a, b) DYNAMO SSA-averaged rainfall (mm day^{-1}) from TRMM 3B42v7 product (solid line) and Q_2 -budget-derived value (dash-dotted line). (c, d) Column net radiation (W m^{-2}) from DYNAMO/CINDY2011/AMIE observation region (breakdown in NSA and SSA) for the aggregation or nonaggregation events. Panels (a) and (c) use SSA only aggregation events. Panels (b) and (d) use all nonaggregation events.

aggregation events experience a similar variability of radiative heating, whereas the amplitude of variability is relatively modest.

5.2 Do these observations show signs of convective self-aggregation?

The aspects of the aggregation events extracted from the present analysis resemble the known characteristics from past numerical studies, including the growth of dry areas in the vicinity of intensifying convection and the resulting enhancement of radiative cooling. On the other hand, dissimilarities are also evident, such as the absence of notable subsidence in the current observations, since the vertical moisture advection does not imply significant drying in the nonprecipitating domain (Fig. 8a). Convective events analyzed in this work are rather limited in number, making it impossible to subsample the data by, for instance, precipitation regimes as done by Tobin et al.

(2012) for a robust interpretation of the results. It is discussed in this section whether the signs of the self-aggregation, as suggested by MICA, are relevant to what we know from the literature, particularly in the contexts of the MJO and of the aggregation time scales.

A vast majority of the aggregation events identified in the current observations occur in the absence of MJO convection, whereas precipitation peaks during active MJO phases are mostly classified as nonaggregation events. A possible explanation for this is that convective aggregation favors a relatively quiescent environment presumably because an intrusion of synoptic-scale disturbances would destroy the large-scale thermodynamic balance required to keep the aggregation in progress (e.g., Wing and Emanuel 2014). In a real atmosphere being constantly disturbed by external dynamic forcing, convective aggregation is unlikely to proceed over an extended period of time as in ide-

alized simulations (e.g., Bretherton et al. 2005). The current finding is at odds with the existing hypothesis that the convective envelope of the MJO may be a manifestation of self-aggregation (Arnold and Randall 2015; see also Holloway et al. 2017). This hypothesis is not necessarily supported by a broad consensus (e.g., Mapes 2016) and has yet to be tested further.

The observed aggregation events evolve over a time scale of about 24 h, which is not surprising given that tropical cloud clusters often have a lifetime of one to two days (Nakazawa 1988). This time scale, however, is substantially shorter than typically seen in RCE simulations of convective self-aggregation (Holloway et al. 2017). The time scale difference is partly due to the fixed spatial scale imposed by the DYNAMO sounding arrays, which may introduce a certain temporal scale of artificial origin. This also explains why the observed aggregation events are disaggregated as quickly while the aggregated state in RCE simulations lasts much longer. Another plausible reason for this discrepancy arises because incessantly disturbed environments hinder the sustainable development of aggregation as mentioned above. Idealized simulations carried out for studying convective aggregation are typically initialized with a homogeneous RCE state, which may inevitably require tens of days until the whole domain is “disturbed” as normally observed in the real atmosphere. The third possibility is that numerical models might not properly simulate physical elements crucial for the rapid evolution of convective aggregation, including, for example, the congestus-mode dynamics fed by cirrus radiative effects (Masunaga and Bony 2018). These issues are largely speculative at this point and are left for future investigations to seek further evidence.

6. Conclusion

In this study, we detected and analyzed convective self-aggregation in real atmosphere on the basis of satellite and field observations. An objectively defined index (MICA) based on satellite infrared imagery, in the same spirit as SCAI (Tobin et al. 2012), was proposed to quantify the degree of convective self-aggregation. The time series of MICA is obtained from Meteosat-7 observations and is related to the thermodynamic fields derived from the DYNAMO/CINDY2011/AMIE sounding-array measurements.

Precipitation events captured during the DYNAMO campaign are categorized with MICA into aggregation and nonaggregation events and are used to contrast the composite time series associated with convective self-aggregation against those without. The temporal

variability of the thermodynamic field accompanying self-aggregation was found to exhibit several features reminiscent of the existing knowledge of convective self-aggregation, although some discrepancies are evident as well. MICA and the number of cloud clusters, a proxy of SCAI, vary over time in a coherent manner. The current observations imply that remarkable aggregation, as suggested by MICA, proceeds within a period of 24 h, substantially shorter than a typical time scale targeted in previous studies on self-aggregation. Otherwise, the characteristics known for self-aggregation, such as drying of a large-scale field, localization of the precipitation area, and enhanced radiative cooling, are present in the observations. A large-scale moisture budget analysis suggests an overall balance between the vertical moisture advection and the apparent moisture sink, while there remains the possibility that the horizontal advection plays a role in transporting moisture between the precipitating domain and adjacent dry area. Although the aspects of the current results suggest possible signs of convective self-aggregation in nature, the present work only opens a long pathway in search for more firm observational evidence to be confirmed in the future. The present study period is limited to the three months of intensive observation of DYNAMO, so the representativeness of the present findings needs to be assessed somewhere else. In the future, it will be interesting to compare the performance of MICA in greater detail in light of other related indices such as SCAI (Tobin et al. 2012), the organization index (Tompkins and Semie 2017), and the COP (White et al. 2018) and the relevant thermodynamic fields on a global, long-term basis.

Acknowledgments

The Meteosat-7 infrared data during the DYNAMO/CINDY2011/AMIE campaign are archived and provided by the DYNAMO Data Archive Center at National Center for Atmospheric Research (NCAR) Earth Observing Laboratory (EOL) (https://www.eol.ucar.edu/field_projects/dynamo). The DYNAMO sounding array data are provided by Colorado State University Mesoscale Dynamics Group and are available online from http://johnson.atmos.colostate.edu/dynamo/products/array_averages/. This work is supported by Japan Society for the Promotion of Science (JSPS) Grants-in-Aid for Scientific Research (KAKENHI) Fund for the Promotion of Joint International Research Development (15KK0157).

References

- Arnold, N. P., and D. A. Randall, 2015: Global-scale convective aggregation: Implications for the Madden-Julian Oscillation. *J. Adv. Model. Earth Syst.*, **7**, 1499–1518.
- Bretherton, C. S., P. N. Blossey, and M. Khairoutdinov, 2005: An energy-balance analysis of deep convective self-aggregation above uniform SST. *J. Atmos. Sci.*, **62**, 4273–4292.
- Coppin, D., and S. Bony, 2015: Physical mechanisms controlling the initiation of convective self-aggregation in a General Circulation Model. *J. Adv. Model. Earth Syst.*, **7**, 2060–2078.
- Hannah, W. M., B. E. Mapes, and G. S. Elsaesser, 2016: A Lagrangian view of moisture dynamics during DYNAMO. *J. Atmos. Sci.*, **73**, 1967–1985.
- Held, I. M., R. S. Hemler, and V. Ramaswamy, 1993: Radiative-convective equilibrium with explicit two-dimensional moist convection. *J. Atmos. Sci.*, **50**, 3909–3927.
- Holloway, C. E., 2017: Convective aggregation in realistic convective-scale simulations. *J. Adv. Model. Earth Syst.*, **9**, 1450–1472.
- Holloway, C. E., A. A. Wing, S. Bony, C. Muller, H. Masunaga, T. S. L'Ecuyer, D. D. Turner, and P. Zuidema, 2017: Observing convective aggregation. *Surv. Geophys.*, **38**, 1199–1236.
- Inoue, K., and L. Back, 2015: Column-integrated moist static energy budget analysis on various time scales during TOGA COARE. *J. Atmos. Sci.*, **72**, 1856–1871.
- Johnson, R. H., and P. E. Ciesielski, 2013: Structure and properties of Madden-Julian oscillations deduced from DYNAMO sounding arrays. *J. Atmos. Sci.*, **70**, 3157–3179.
- Maddox, R. A., 1980: Mesoscale convective complexes. *Bull. Amer. Meteor. Soc.*, **61**, 1374–1387.
- Mapes, B. E., 2016: Gregarious convection and radiative feedbacks in idealized worlds. *J. Adv. Model. Earth Syst.*, **8**, 1029–1033.
- Masunaga, H., 2015: Assessment of a satellite-based atmospheric budget analysis method using CINDY2011/DYNAMO/AMIE and TOGA COARE sounding array data. *J. Meteor. Soc. Japan*, **93A**, 21–40.
- Masunaga, H., and S. Bony, 2018: Radiative invigoration of tropical convection by preceding cirrus clouds. *J. Atmos. Sci.*, **75**, 1327–1342.
- Muller, C. J., and I. M. Held, 2012: Detailed investigation of the self-aggregation of convection in cloud-resolving simulations. *J. Atmos. Sci.*, **69**, 2551–2565.
- Nakazawa, T., 1988: Tropical super clusters within intraseasonal variations over the western Pacific. *J. Meteor. Soc. Japan*, **66**, 823–839.
- Roca, R., and V. Ramanathan, 2000: Scale dependence of monsoonal convective systems over the Indian Ocean. *J. Climate*, **13**, 1286–1298.
- Ruppert, J. H., Jr., and R. H. Johnson, 2015: Diurnally modulated cumulus moistening in the preonset stage of the Madden-Julian Oscillation during DYNAMO. *J. Atmos. Sci.*, **72**, 1622–1647.
- Sherwood, S. C., 1999: Convective precursors and predictability in the tropical western Pacific. *Mon. Wea. Rev.*, **127**, 2977–2991.
- Stein, T. H. M., C. E. Holloway, I. Tobin, and S. Bony, 2017: Observed relationships between cloud vertical structure and convective aggregation over tropical ocean. *J. Climate*, **30**, 2187–2207.
- Tobin, I., S. Bony, and R. Roca, 2012: Observational evidence for relationships between the degree of aggregation of deep convection, water vapor, surface fluxes, and radiation. *J. Climate*, **25**, 6885–6904.
- Tobin, I., S. Bony, C. E. Holloway, J.-Y. Grandpeix, G. Sèze, D. Coppin, S. J. Woolnough, and R. Roca, 2013: Does convective aggregation need to be represented in cumulus parameterizations? *J. Adv. Model. Earth Syst.*, **5**, 692–703.
- Tompkins, A. M., 2001: Organization of tropical convection in low vertical wind shears: The role of water vapor. *J. Atmos. Sci.*, **58**, 529–545.
- Tompkins, A. M., and A. G. Semie, 2017: Organization of tropical convection in low vertical wind shears: Role of updraft entrainment. *J. Adv. Model. Earth Syst.*, **9**, 1046–1068.
- White, B. A., A. M. Buchanan, C. E. Birch, P. Stier, and K. J. Pearson, 2018: Quantifying the effects of horizontal grid length and parameterized convection on the degree of convective organization using a metric of the potential for convective interaction. *J. Atmos. Sci.*, **75**, 425–450.
- Wing, A. A., and K. A. Emanuel, 2014: Physical mechanisms controlling self-aggregation of convection in idealized numerical modeling simulations. *J. Adv. Model. Earth Syst.*, **6**, 59–74.
- Wing, A. A., K. Emanuel, C. E. Holloway, and C. Muller, 2017: Convective self-aggregation in numerical simulations: A review. *Surv. Geophys.*, **38**, 1173–1197.
- Yanai, M., S. Esbensen, and J.-H. Chu, 1973: Determination of bulk properties of tropical cloud clusters from large-scale heat and moisture budgets. *J. Atmos. Sci.*, **30**, 611–627.
- Yoneyama, K., C. Zhang, and C. N. Long, 2013: Tracking pulses of the Madden-Julian oscillation. *Bull. Amer. Meteor. Soc.*, **94**, 1871–1891.